Electronic Supplementary Material (ESI) for Physical Chemistry Chemical Physics.

Supplementary Information

Metastability of Palladium Carbide Nanoparticles during Hydrogen Release from Liquid Organic Hydrogen Carriers

Ralf Schuster,[a] Manon Bertram,[a] Henning Runge,[b] Simon Geile,[b] Simon Chung,[b] Vedran Vonk,[b] Heshmat Noei,[b] Agnieszka Poulain,[c] Yaroslava Lykhach,*[,a] Andreas Stierle,[b,d] and Jörg Libuda*[,a]

[a] *Interface Research and Catalysis, Erlangen Center for Interface Research and Catalysis, Friedrich-Alexander-Universität Erlangen-Nürnberg, Egerlandstraße 3, 91058 Erlangen, Germany*

[b] *Deutsches Elektronen-Synchrotron DESY, Notkestrasse 85, 22607 Hamburg, Germany*

[c] *European Synchrotron Radiation Facility, 71 Avenue des Martyrs, 38000 Grenoble, France*

[d] *Fachbereich Physik, Universität Hamburg, Jungiusstrasse 11, 20355 Hamburg, Germany*

*corresponding authors: yaroslava.lykhach@fau.de; joerg.libuda@fau.de

S1. XRR analysis

The total amount of Pd on the sample containing big (15 nm) nanoparticles was determined by means of XRR analysis. The nominal thickness of Pd film was 2.39 nm.

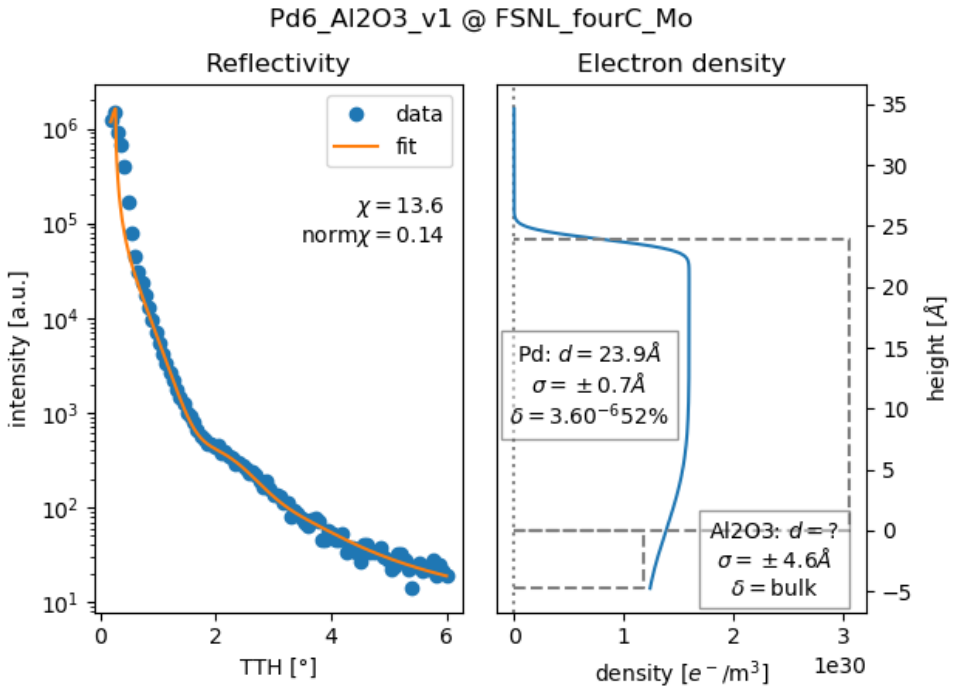

Figure S1. X-ray scattering intensity (left) and electron density profile (right) obtained from the $Pd/Al_2O_3(0001)$ sample containing big (15 nm) Pd nanoparticles.

S2. Size distribution and particle density

The size distribution and particle density on the $Pd/Al_2O_3(0001)$ sample containing big (15 nm) nanoparticles were studied by means of SEM before and after reaction with MCH at 500 K (Figure S2). The Gaussian size distribution on as-prepared $Pd/Al_2O_3(0001)$ sample yielded average diameter of Pd nanoparticles of 14.2 nm with a Full Width at Half Maximum (FWHM) of 7 nm (Figure S2 a-b). After the reaction with MCH, the corresponding average diameter of Pd nanoparticles increased to 19.2 nm and the size distribution significantly broaden resulting in FWHM of 15.7 nm (Figure S2 c-d).

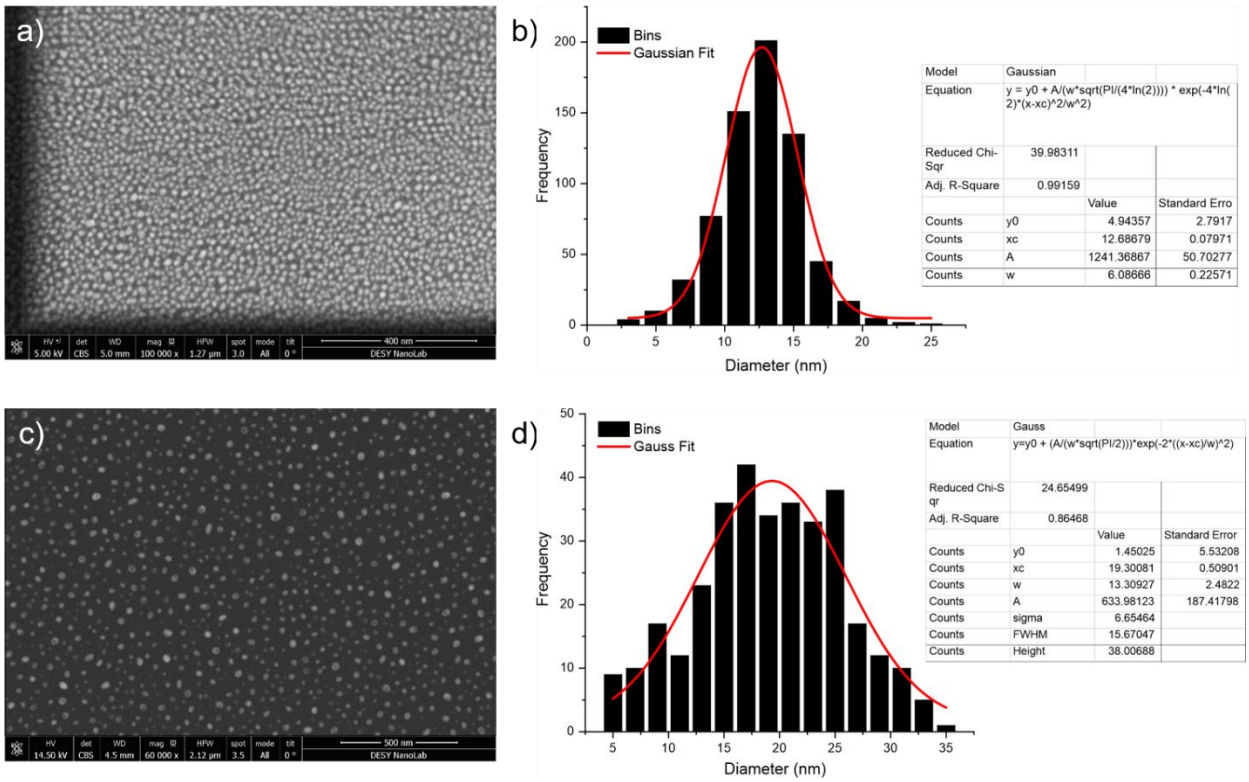

Figure S2. SEM images (a, c) and the size distribution of Pd nanoparticles (b, d) obtained from the Pd/Al_2O_3(0001) sample containing big Pd nanoparticles before (a-b) and after (c-d) the reaction with MCH.

S3. Comparison of the Pd_xC evolution

We plotted the evolution of fractions of palladium carbides, Pd_xC and Pd_6C, obtained upon exposure of the Pd/Al_2O_3(0001) samples containing small (SP) and big (BP) Pd nanoparticles to MCH at low (LF) and high (HF) flow rates on the same time scale for easier comparison in Figure S3.

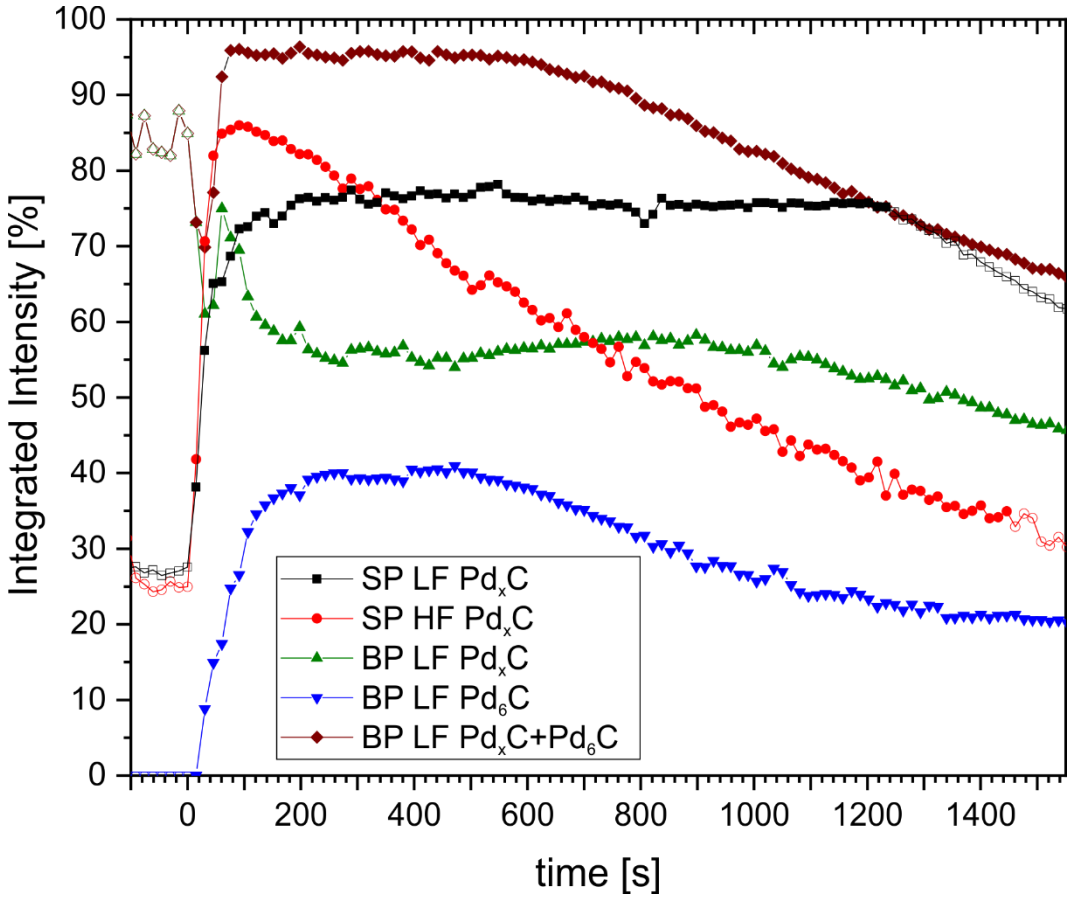

Figure S3. Fractions of Pd_xC obtained upon exposure of the $Pd/Al_2O_3(0001)$ samples containing small (SP) and big (BP) Pd nanoparticles to MCH at low (LF) and high (HF) flow rates. For big Pd nanoparticles, we added the contribution from Pd_6C and total Pd_xC + Pd_6C contribution. Full and empty symbols correspond to the MCH and Ar exposures, respectively.

S4. Structure of 15 nm Pd nanoparticles

A two-dimensional (2D) diffraction map obtained from 15 nm Pd nanoparticles supported on α-$Al_2O_3(0001)$ under exposure to Ar flow at 500 K at the flow rate of 5 ml/min is shown in Figure S4a. Two types of diffraction patterns were observed including a Bragg reflection spot and a Debye-Scherrer ring. The intensity profiles of the Bragg spot and the Debye-Scherrer ring were obtained along the azimuthal lines (i) and (ii), respectively.

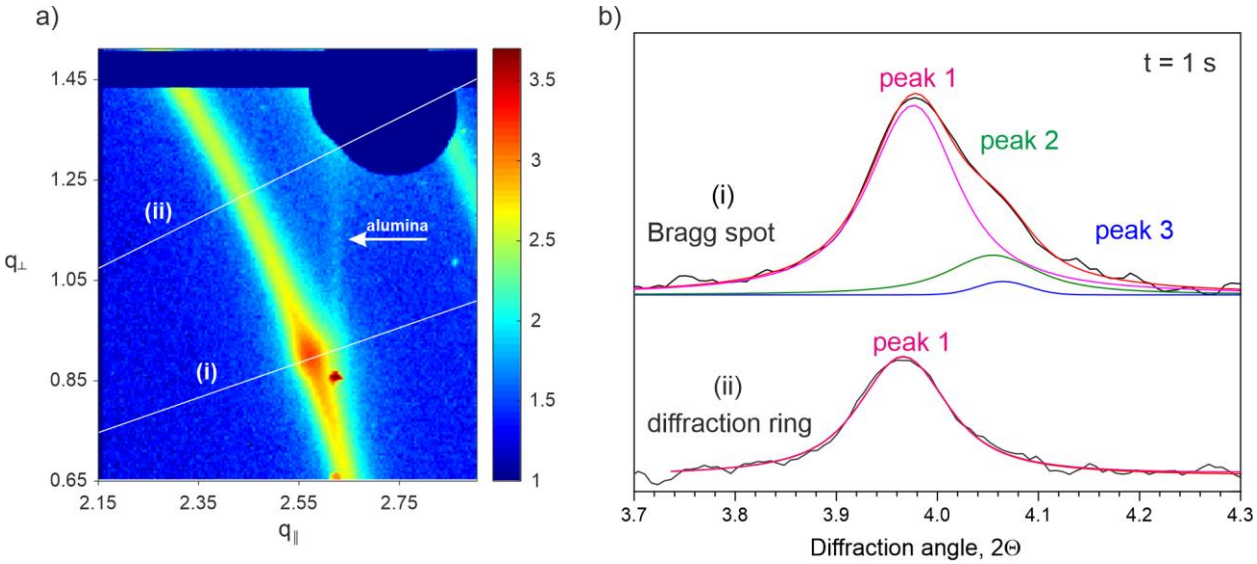

Figure S4. 2D reciprocal map (a) and intensity profiles (b) along the radial lines (i) and (ii) obtained under Argon at t=1 s.

The intensity profile of the Debye-Scherrer ring (ii) was fitted with a single peak (peak 1) at the diffraction angle of 3.966°. In contrast, three peaks were resolved in the intensity profile of the Bragg spot at 3.976° (peak 1), 4.055° (peak 2), and 4.065° (peak 3). Among these, the peaks 1 and 2 originate from two different phases of Pd nanoparticles. Based on the value of the diffraction angle, we associate peak 2 with the clean Pd phase. The smaller diffraction angle of peak 1 suggests an expansion of the Pd lattice due carbon incorporation. Therefore, we associate the peak 1 with the Pd_xC phase, i.e. a solid solution of carbon in Pd. Peak 3 corresponds to the overlapping signal from the α-Al_2O_3(0001) substrate. During fitting, the position of peak (3) was fixed and its intensity was allowed to vary by ±20%.

S5. Evolution of the Debye-Scherrer ring

The evolution of the intensity and the position of peak 1 from the Debye-Scherrer ring during period of time between 0 and 350 s is shown in Figure S5. This period includes the time under Argon (0-190 s) and the beginning of exposure to MCH (from 190 s). The shift of peak (1) is accompanied by the increase of its intensity.

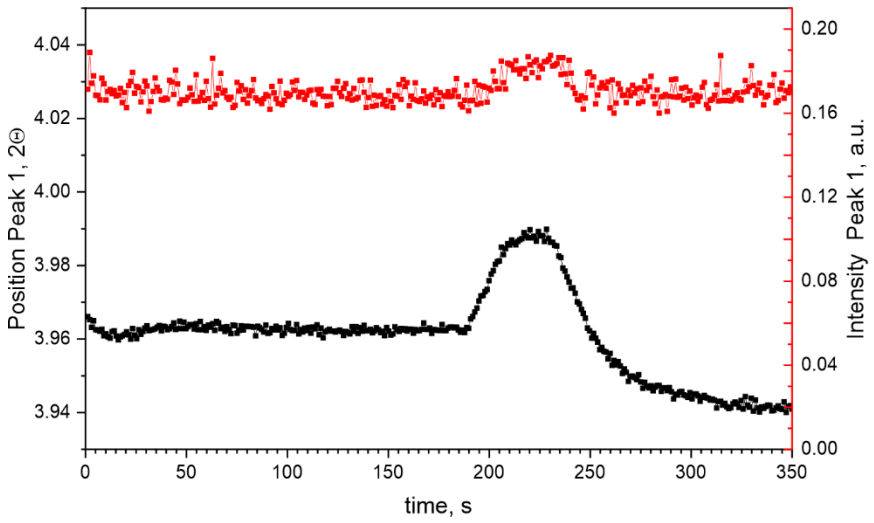

Figure S5. The position (black) and the intensity (red) of peak (1) from the Debye-Scherrer ring as a function of time.

Under exposure to MCH flow, peak 1 shifts to higher diffraction angles between 190 and 225 s, then, to lower angles between 225 and 350 s and remains nearly constant afterwards. A new peak (peak 2) appears at about 4.006° and grows at the expense of the peak 1 between 1000 and 2200 s (see Figure S6). This new peak gradually shifts to the position of 4.03°. According to the diffraction angle value, the new peak 2 corresponds to the clean Pd phase (similar as in the Bragg spot). The observed behavior suggests that the pure Pd phase forms at the expense of Pd_xC due to segregation of carbon to the surface of supported Pd nanoparticles.

In order to achieve higher fitting accuracy, we included the second diffraction ring at diffraction angles 4.4°-4.8° into the fitting envelope. During the fitting, we kept the distances between the corresponding pairs of peaks in the first and second diffraction rings the same.

The corresponding 2D diffraction maps are shown in Figure S6. It can be seen that the diffraction ring first broadens (t=1522.4 s) and then splits into two rings (t=3653.6 s). The observed splitting in the Debye-Scherrer ring indicates the presence of two well-defined phases: Pd_6C and pure Pd represented by peaks 1 and 2, respectively. Note that the Pd_6C phase correspond to Pd_xC with the maximum content of carbon (about 14%).

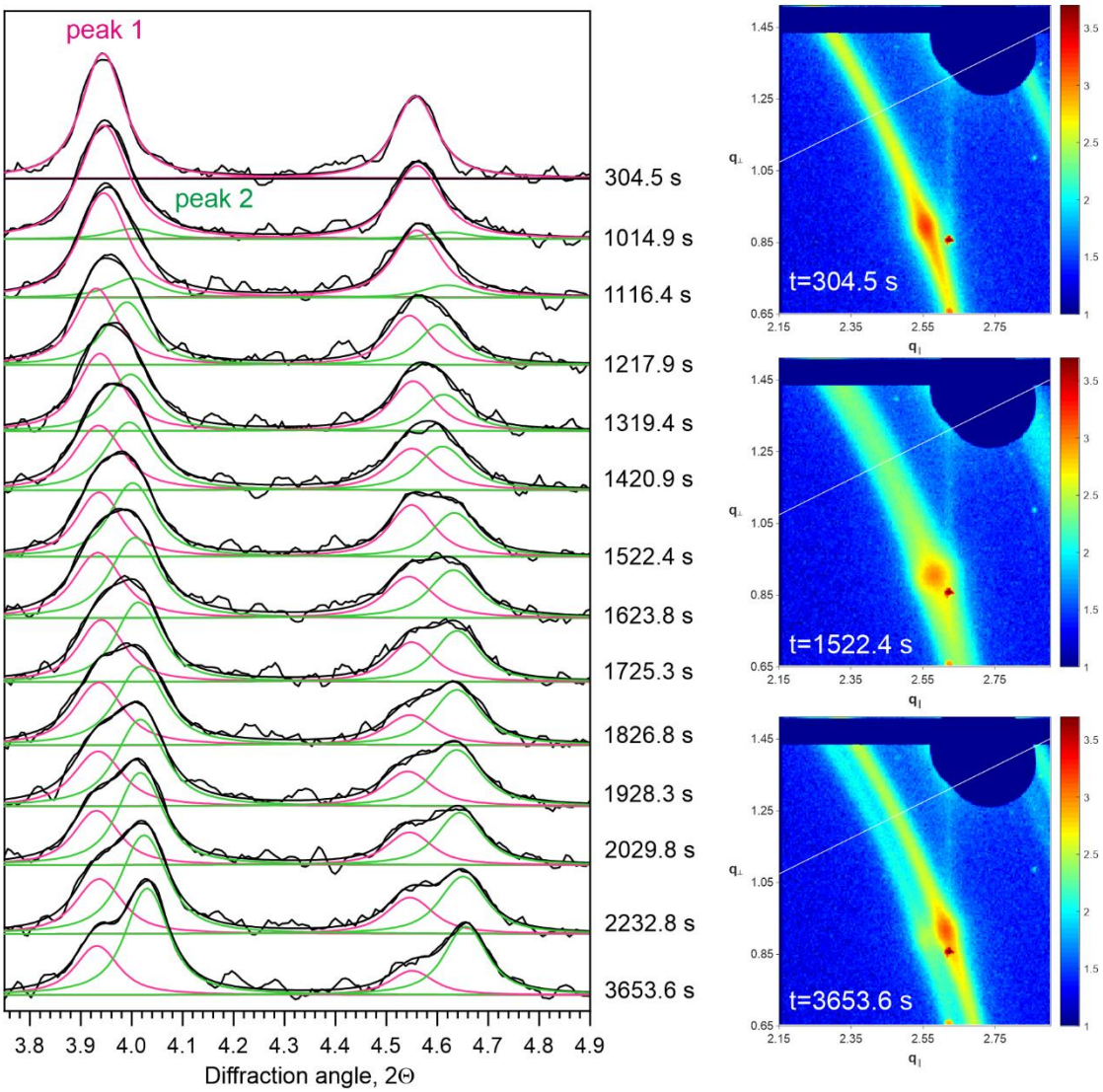

Figure S6. Intensity profiles of the Debye-Scherrer ring and selected 2D reciprocal maps obtained under the exposure to MHC between 300 and 3660 s.

The evolution of the intensities of peak 1 and peak 2 from the Debye-Scherrer ring are plotted in Figure S7. The grey box indicates the exposure period to MCH. One can see that the phase composition of the Pd nanoparticles started to change after a short period of time under the exposure to MCH.

Surprisingly, the phase composition formed under the exposure to MCH remains stable for some time in Argon atmosphere. The decomposition of carbide starts when peak 1 grows at the expense of peak 2 (~4500 s) and shifts to the position observed at t=1 s. The observed behavior is consistent

with the transformation of Pd_6C into Pd_xC accompanied by segregation of carbon to the surface of Pd nanoparticles driven by the growth of graphene/graphite.

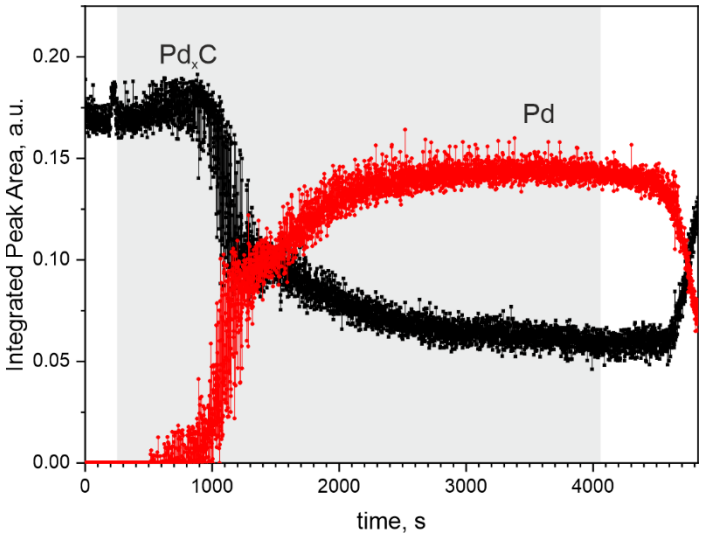

Figure S7. The intensities of peak (1) and peak (2) from the Debye-Scherrer ring as a function of time. The grey box indicates time under exposure to MCH.

S5. Comparison of the intensity profiles of the Bragg spot and Debye-Scherrer ring

As shown in Figure S4, peak 1 from the Bragg spot is located at a very similar diffraction angle as peak 1 from the Debye-Scherrer ring. Therefore, we assume that peak 1 from the Bragg spot is associated with the PdC_x phase with similar structural parameters. The difference in the compositions of the epitaxial and non-epitaxial nanoparticles is related to the existence of the pure Pd phase (peak 2) in the epitaxial Pd nanoparticles.

First, we discuss the positions of the peaks in the period of time 0-350 s (Figure S8). We observed that peak 1 from the Bragg spot shifts in parallel to peak 1 from the Debye-Scherrer ring. In particular, between 190 and 230 s, both peaks shift to higher diffraction angles and reach the same value of 3.99°.

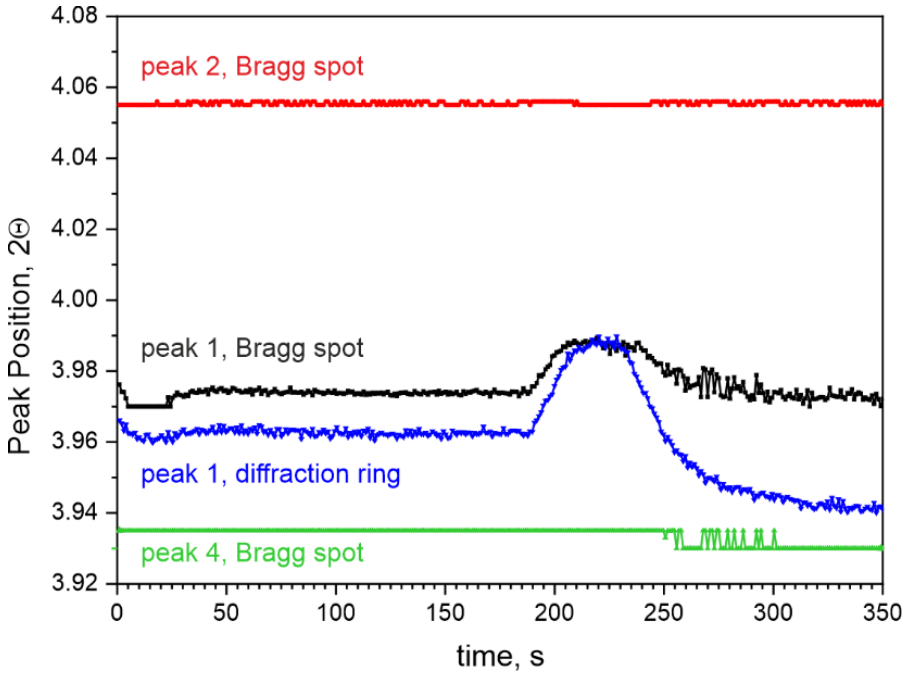

Figure S8. Comparison of the peak positions from the Bragg spot and the Debye-Scherrer ring as a function of time.

Above 230 s, peak 1 from the Debye-Scherrer ring and peak 1 from the Bragg spot both shift to lower diffraction angles. However, peak 1 from the Debye-Scherrer shifts more rapidly. At 350 s, peak 1 from the Debye-Scherrer and peak 1 from the Bragg spot approach the diffraction angles of 3.94° and 3.97°, respectively. As a result, the distance between peak 1 from the Debye-Scherrer ring and peak 1 from the Bragg spot increase significantly. At about 250 s, a new peak, peak 4, emerges in the intensity profile of the Bragg spot at about 3.93°.

The intensity profiles obtained at t=304.5 s are shown in Figure S9. By comparing the profiles from the Bragg spot and the Debye-Scherrer ring, one can see that peak 4 in the Bragg spot and peak 1 in the Debye-Scherrer ring both represent the Pd_6C phase. However, the difference between the epitaxial and non-epitaxial Pd nanoparticles is that the non-epitaxial Pd nanoparticles are composed of a single Pd_6C phase while the epitaxial nanoparticles contain two phases, Pd_6C and Pd_xC.

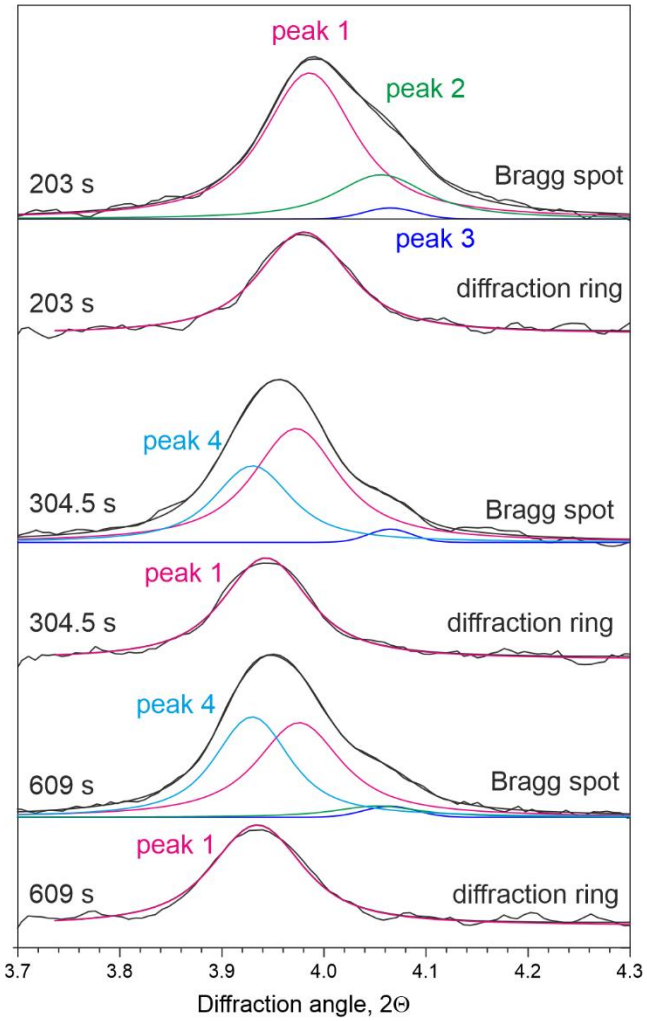

Figure S9. Comparison of the intensity profiles of the Bragg spot and the Debye-Scherrer ring.

Peak 2 in the Debye-Scherrer ring (assigned to pure Pd, see above) emerges above 800 s. At the same time, peak 2 from the Bragg spot grows and dominates the intensity profile at 3653.6 s (see Figure S10).

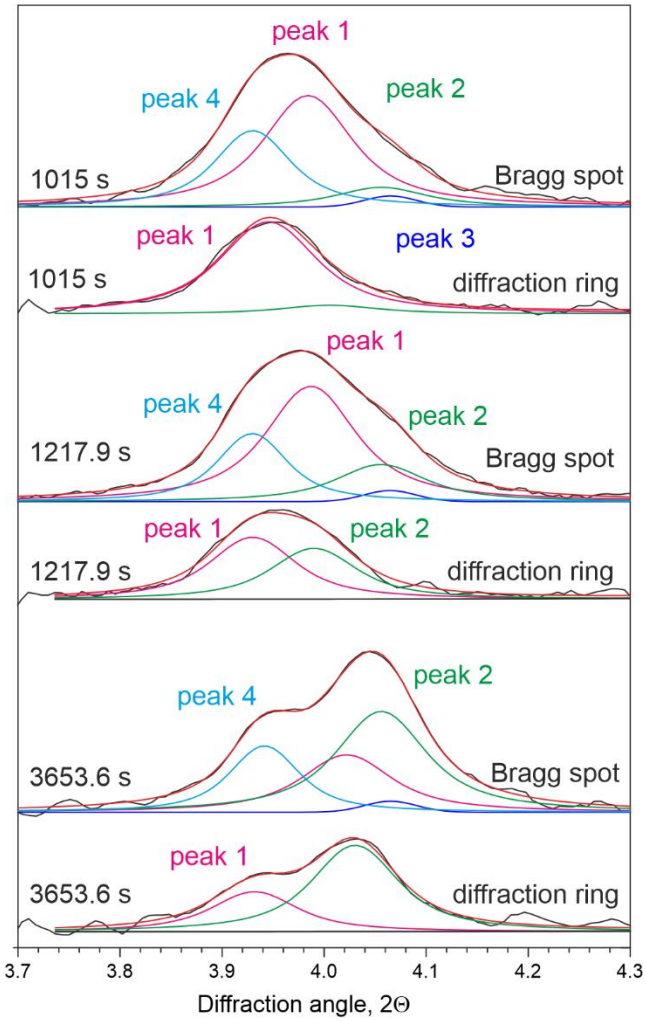

Figure S10. Comparison of the intensity profiles of the Bragg spot and the Debye-Scherrer ring.

The intensity profiles obtained from 8.1 nm Pd/Al_2O_3(0001) under Ar flow at t=4826 s are compared in Figure S11. One can see that the intensity profiles of both the Bragg spot and the Debye-Scherrer ring contain the contributions from Pd_xC and pure Pd. This observation suggests that the phase composition of both epitaxial and non-epitaxial Pd nanoparticles is similar.

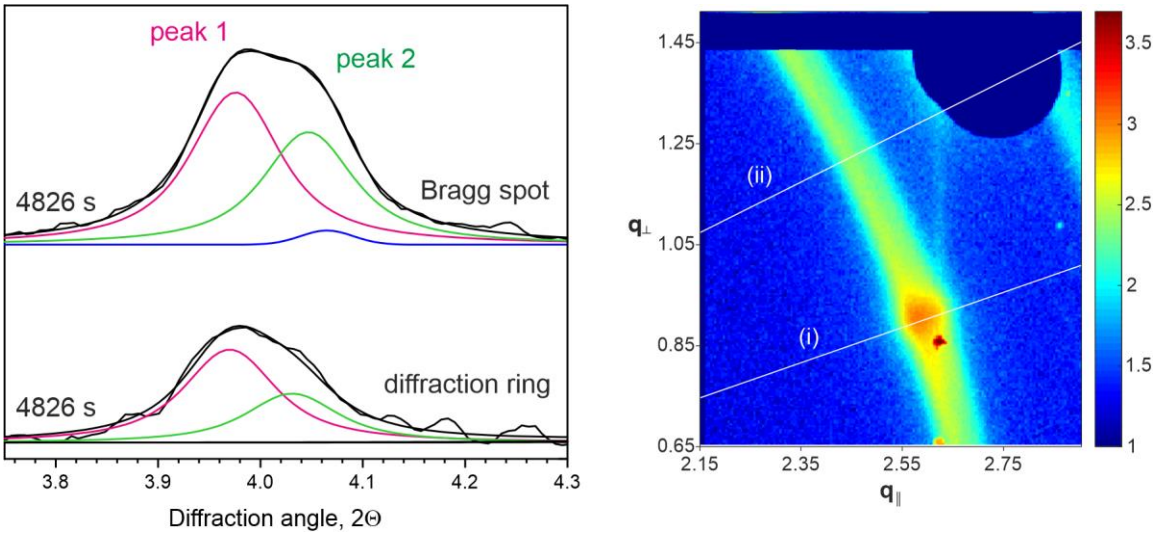

Figure S11. Comparison of the intensity profiles of the Bragg spot and the powder ring.

Conclusions

The comparison of the radial intensity profiles of the Bragg spot and the Debye-Scherrer ring revealed a partial overlap between the contributions. This leads to an enhancement of particular phase contributions in the intensity profiles of the Bragg spot:

1) The Pd_6C contribution in the Bragg spot (peak 4) overlaps with the corresponding contribution in the Debye-Scherrer ring (peak 1) between 250 and 4400 s.

2) The Pd_xC contribution in the Bragg spot (peak 1) overlaps with the contribution from pure Pd in the Debye-Scherrer ring (peak 2) between 1000 s and 4400 s.

3) The pure Pd contribution in the Bragg spot (peak 2) overlaps with the corresponding contribution in the Debye-Scherrer ring (peak 2) between 4400 and 4826 s.